High-Performance Aminated Poly(phenylene sulfide)/ZnO Nanocomposites for Medical Applications

Ana M. Díez-Pascual*[,†] and Angel L. Díez-Vicente[‡]

[†]Institute of Polymer Science and Technology (ICTP-CSIC), Juan de la Cierva 3, 28006, Madrid, Spain
[‡]Airbus Operations S. L., John Lennon s/n, 28906 Getafe, Madrid, Spain

Ⓢ *Supporting Information*

ABSTRACT: An aminated poly(phenylene sulfide) derivative (PPS-NH$_2$) has been melt-blended with different contents of ZnO nanoparticles, and the morphology, thermal, mechanical, tribological, antibacterial, and dielectric properties of the resulting nanocomposites have been investigated. The nanoparticles were dispersed within the matrix without the need for surfactants or coupling agents. A gradual rise in the crystallization temperature and the degree of crystallinity was found with increasing ZnO loading, confirming that the nanoparticles act as nucleating agents for PPS-NH$_2$ crystallization. The nanoparticles reduced the water absorption and strongly increased the thermal stability of the matrix, leading to an extraordinary increase in the initial degradation temperature of 80 °C at 8.0 wt % nanoparticle content. The results showed that the stiffness, strength, toughness, glass transition, and heat distortion temperature were remarkably enhanced, whereas the coefficient of thermal expansion decreased upon addition of ZnO, ascribed to strong hydrogen bonding interactions between the amino groups of the matrix and the hydroxyl moieties of the nanoparticles. Moreover, the nanocomposites retained the tensile properties after being exposed to several cycles of steam sterilization. More importantly, an unprecedented drop in wear rate of nearly 100-fold was attained in the nanocomposite with the highest loading, demonstrating the suitability of these nanoparticles for providing wear resistance to the matrix. All the nanocomposites displayed low dielectric constant and dielectric loss, hence can be employed as insulating materials in electrosurgical applications. They also exhibited active inhibition against both Gram-positive and Gram-negative bacteria, which was gradually enhanced with increasing ZnO content. These nanocomposites are suitable as lightweight high-performance materials in the field of medicine and dentistry.

KEYWORDS: PPS derivative, ZnO nanoparticles, thermomechanical properties, antibacterial activity, minimally invasive surgery
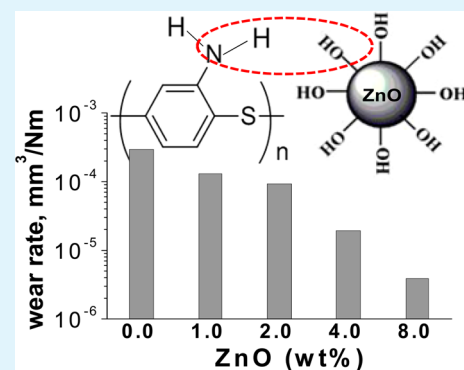
1. INTRODUCTION

Over the last years, the addition of small amounts of inorganic nanoparticles to a polymer matrix has become a very promising route to attain novel materials with enhanced behavior due to synergistic effects.[1] The nanocomposite properties are conditioned by the nanofiller characteristics (shape, size, roughness, etc.), its dispersion and interfacial adhesion with the host matrix.[2] The most important advantages of nanofillers are their high specific surface area that leads to a better bonding between the two phases, their higher density and surface energy in comparison to microparticles; therefore, only low nanofiller loadings (1–10 wt %) are needed to achieve properties similar to or even superior than those obtained using traditional microfiller contents (15–40 wt %).[3] In this regard, various types of inorganic nanoparticles are being employed, including metal oxides (ZnO, TiO$_2$, Al$_2$O$_3$, CaCO$_3$, etc.), clays (montmorillonite, hectorite, saponite), silica (SiO$_2$), silicon carbide (SiC), and transition metal chalcogenides (MoS$_2$,WS$_2$, etc.), among others.[3–7]

Traditionally, thermoplastic nanocomposites have been used to replace metallic materials in engineering applications subjected to high stress, friction, and/or wear because of their superior performance combined with reduced weight and excellent corrosion resistance. Recently, the use of these nanocomposites has been extended to the field of medical technology, for applications including orthotic and prosthetic devices, sterilization containers, instruments for diagnostic purposes, products for therapeutic treatment, equipment for intensive care, materials used in devices for dental tartar removal or to harden fillings, and so forth.[8] Thermoplastic nanocomposites play a key role in important areas where the combination of lightweight, high stiffness/strength, chemical and sterilization resistance, good dielectric properties, dimensional stability, transparency, low water absorption, precision, and good machining properties is desired. One of the challenges in modern surgery is the development of miniaturized tools that allow for less invasive methods and enable the access to areas difficult to reach within the human body. This trend toward minimally invasive surgery (MIS), surgical procedures that do not require large incisions, has

generated an increasing demand for lightweight precision microsized instruments that are currently implemented in a wide range of medical fields such as gynecology, urology, and cardiothoracic surgery.[9] MIS often requires a small incision that enables the passage of a small-diameter tube inside the body through which probes (i.e., cauterization devices, light sources or miniaturized TV camera lens) and/or microsized surgical tools can be introduced. This new approach considerably diminishes postoperative pain and recuperation time, and simultaneously enhances cosmetic outcome and overall cost-effectiveness.[10] A variety of thermoplastic materials such as filler-reinforced poly(ether ether ketone) (PEEK), polyamide 6 (PA-6), poly(ether imide) (PEI) and poly(phenylene sulfide) (PPS) are currently being developed to comply with the rigorous demands of medical technology.[11,12]

PPS is a semicrystalline engineering thermoplastic with a symmetrical rigid backbone chain composed of para-substituted phenylene rings and sulfur atoms. It presents outstanding physical and chemical properties such as high thermal stability, high deflection temperature, excellent mechanical and friction properties, resistance to common organic solvents below 200 °C, dimensional stability over wide variations of temperature and moisture, flame retardancy, antiaging, and precision moldability, currently used in a wide variety of sectors ranging from the automobile and aerospace to the electronics, appliance, and chemical industries.[13] Recently, high-purity PPS has also been employed in the field of medicine.[11] However, certain uses of this thermoplastic have been somewhat limited because of its relatively low T_g compared to its high T_m, its brittleness and electrically insulating character. In addition, it is insoluble in common organic solvents, which represents the main obstacle for its functionalization, hence the ability to interact with other substances.[14] In this regard, chemical modifications of PPS are interesting strategies to prepare derivatives with a small amount of polar reactive functional groups suitable to interact with other molecules through covalent or hydrogen bonding, to be further integrated in composite materials.[14−16] The aromatic rings of the polymer backbone are crucial for its functionalization because they can act as an electron source for electrophilic substitution reactions.[14] Halogenation reactions are typically carried out via in situ polymerization of monomers in selected solvents.[17] However, these methods are difficult to scale-up since involve several reaction steps and specific monomers should be used to synthesize polymers with a high molecular weight. On the other hand, sulfonation reactions are not appropriate because of their reversibility. Consequently, the aromatic nitration seems to be the most suitable route to functionalize this thermoplastic.

Zinc oxide (ZnO) nanostructures are multifunctional inorganic semiconductors that have drawn enormous attention over recent years due to their extraordinary characteristics for optics, photonics and electronics.[18] They exhibit intensive ultraviolet absorption and marked antibacterial activity at pH values in the range of 7−8 even in the absence of light,[19] and hence are widely used for optical devices and antimicrobials. Further, these low cost, nontoxic and biocompatible nanofillers possess outstanding mechanical properties,[20] high thermal conductivity and low coefficient of thermal expansion, hence are highly suitable as nanofillers in polymer composites. Thus, ZnO nanoparticles have been found to be effective for reducing the wear rate of PEEK[21] and ultrahigh-molecular-weight polyethylene UHMWPE,[22] and improving the mechanical

performance of high-density polyethylene (HDPE)[23] and PA-6.[24] To prevent nanoparticle aggregation, some of these works modified the surface of ZnO nanoparticles with silane coupling agents. However, these agents are very expensive, water sensitive, and require specific functional groups in the polymer matrix to ensure good interaction. ZnO nanoparticles with different sizes and shapes can be prepared by various methods including hydrothermal synthesis, thermal evaporation, electrochemical decomposition, sol−gel, sonochemical technique, and so forth.[25−27]

To date, very scarce literature regarding the preparation and characterization of PPS/ZnO nanocomposites has been published. Bahadur and Sunkara[28] investigated the tribological behavior of PPS composites reinforced with nanoscale particles of TiO_2, ZnO, CuO, and SiC. The wear rate of the matrix was found to decrease when TiO_2 and CuO were used as fillers, albeit increased upon addition of ZnO and SiC due to poor nanoparticle dispersion and the formation of a discontinuous and weakly adhered transfer film on the countersurface. To overcome these drawbacks, an aminated polymer derivative (PPS-NH$_2$) has been used in the present work as matrix material for the development of the nanocomposites. The derivative was prepared in a one-pot reaction through a simple and economic method, easy to scale-up.[14] Further, it should exhibit higher hydrophilicity compared to the parent PPS, hence improved compatibility with the nanofillers. Raw ZnO nanoparticles at various loadings have been incorporated in this polymer derivative following a manufacturing process based on conventional melt-blending and compression molding, without the aid of surfactants or coupling agents. An extensive characterization has been carried out to analyze in detail the influence of the nanoparticles on the morphology, thermal, mechanical, dielectric, tribological, and antibacterial properties of these novel nanocomposites with a view to use them for lightweight precision instruments in the fields of medicine and dentistry.

2. EXPERIMENTAL SECTION

Materials. PPS (TECATRON) was supplied by Ensinger Inc. in powder form. This high purity grade, with excellent thermal and chemical resistance, complies with USP class VI and ISO 10993 requirements specified for plastics used for medical applications, and presents the following physical characteristics: $d_{25\ °C} = 1.35$ g/cm^3, $T_g \approx 90$ °C, $T_m \approx 282$ °C. The polymer was dried at 100 °C for 14 h and stored in a dry atmosphere. The aminated derivative (PPS-NH$_2$) was synthesized from a nitrated polymer (PPS-NO$_2$) using sodium dithionite as reduction agent.[14] To assess the optimal functionalization degree (FD) of PPS-NH$_2$, five derivatives with FD in the range of 10−86% were initially prepared. A derivative with a FD of ∼18% (as determined by elemental analysis) was selected as matrix for the development of the nanocomposites due to its optimum balance between stiffness, thermal stability, coefficient of friction and number of functional groups. The derivative was purified by continuous extraction in a Soxhlet apparatus with distilled water for 24 h and finally dried in an oven at 80 °C. Zinc oxide nanopowder, <100 nm size and specific surface area between 15 and 25 m^2/g, was supplied by Sigma-Aldrich.

Preparation of PPS-Based Nanocomposites. Prior to composite manufacturing, ZnO nanoparticles and the PPS-NH$_2$ powder were dispersed in ethanol by ultrasonication for 30 min, and subsequently dried in vacuum at 50 °C until the solvent was completely evaporated. The melt-compounding of the resulting dispersions was performed in a Thermo-Haake MiniLab microextruder operating at 320 °C, with a screw speed of 150 rpm for 20 min. Four composites were prepared, with ZnO contents of 1.0, 2.0, 4.0, and 8.0 wt %, respectively. For

comparative purposes, reference nanocomposites based on a PPS matrix reinforced with the same amounts of nanoparticles were manufactured under identical conditions. Prior to characterization, the nanocomposites were pressed into thin films (~1 and 3 mm thick), and annealed for 2 h at 180 °C. The films displayed a smooth surface (R_a < 4 μm).

Characterization Techniques. The morphology of the nanocomposites was investigated using a SU8000 Hitachi scanning electron microscope (SEM).[21] Transmission electron microscopy (TEM) images were acquired with a Philips Tecnai 20 FEG (LaB$_6$ filament) electron microscope fitted with an EDAX detector.[29]

A PerkinElmer Spectrum One spectrometer equipped with a Universal ATR sampling accessory (diamond crystal) and a red laser excitation source (632.8 nm) was used to obtain the room temperature (RT) attenuated total reflectance FT-IR spectra.[21] The thermal stability of the composites was analyzed by thermogravimetric analysis (TGA) using a TA Instruments Q50 thermobalance at a heating rate of 10 °C/min.[21] X-ray diffractograms (XRD) were recorded at RT with a Bruker D8 Advance diffractometer using a Cu tube as X-ray source (λ CuKα = 1.54 Å).[21] The degree of crystallinity X_c was estimated from the diffractograms using the relation: $X_c = I_c/(I_c + I_a)$, where I_a and I_c are the integrated intensities of the amorphous and crystalline phases, respectively.

Dynamic differential scanning calorimetry (DSC) measurements were carried out on a Mettler DSC 30. Samples were melted at 320 °C and maintained at this temperature for 5 min to eliminate the thermal history of the material. Then, they were cooled to 30 °C and reheated to 320 °C, all the steps at a rate of 10 °C/min. The crystallization enthalpy was used to estimate the level of crystallinity of the samples.

To determine the water absorption, samples were dried in a desiccator at 0% relative humidity (RH) for 1 week. Subsequently, they placed in a beaker at 100% RH and allowed to absorb water until a constant weight was attained. Water uptake was calculated as $[(W_f - W_i)/W_i]100$, where W_i and W_f are the initial and final (equilibrium) weight of the samples, respectively. Five replicates for each sample were measured, and the average value is reported.

The dynamic mechanical performance was investigated with a Mettler DMA861 dynamic mechanical analyzer,[21] in the range of −115 to 200 °C. Tensile tests were carried out using an INSTRON 4204 mechanical tester at RT and 50 ± 5% RH, with a crosshead speed of 1 mm/min and a load cell of 1 kN.[21] Tensile measurements were also performed on composites subjected to 10 steam sterilization cycles in an autoclave in which they were exposed to saturated steam for 15 min at 121 °C and 2 bar, following the EN ISO 17665 standard.

Heat distortion temperature (HDT) measurements were carried out using a TA 2980 DMA tester following the ASTM D648 standard. Specimens were conditioned at 25 ± 2 °C and 50 ± 5% RH for 48 h prior to the tests. Samples were heated from RT to 250 °C at a rate of 2 °C/min under a load of 1.8 MPa. The coefficient of thermal expansion (CTE) was determined by thermomechanical analysis (TMA) using a Perkin−Elmer TMA 7 instrument. Samples were dried for 1 h at 100 °C and then cooled in a desiccator. Subsequently, they were heated from 0 to 200 °C at rate of 2 °C/min under a nitrogen atmosphere, and the CTE was determined from the slope of the TMA expansion curve at 25 °C. Pin-on-disk tests were performed at 24 ± 2 °C and 22 ± 2% RH on a Microtest MT 400−98 apparatus, using a 6 mm diameter 100Cr6 steel ball like pattern slide.[21]

The antibacterial activity was evaluated against Gram-positive *Staphylococcus aureus* (*S. aureus*, ATCC 12600) and Gram-negative *Escherichia coli* (*E. coli*, ATCC 25922) bacteria.[21] Experiments were carried out without exposure to UV light. The samples were submerged in a nutrient broth of ~2.0 × 10^6 colony forming units per ml (CFU/ml). After incubation at 37 °C for 24 h, the survival ratio (SR) was calculated following the equation: SR (%) = (N/N$_o$) × 100, where N_o and N are the average number of microorganisms on the neat polymer and the nanocomposites, respectively.

The dielectric properties of the nanocomposites were measured with an HP 4294 impedance analyzer in the frequency range between 10 and 1 × 10^6 Hz at room temperature.

3. RESULTS AND DISCUSSION

FT-IR Study. The ATR-FTIR spectra of ZnO, PPS, the aminated derivative and the nanocomposites with 2.0 and 8.0 wt % loading were recorded to obtain information about the nanoparticle−polymer interactions (Figure 1). The spectrum of
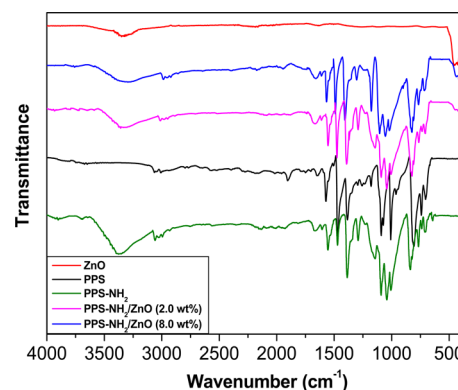

Figure 1. FT-IR spectra of ZnO, neat PPS, PPS-NH$_2$, and the nanocomposites with 2.0 and 8.0 wt % nanoparticle loading.

ZnO shows a broad peak centered at 3350 cm^{-1} assigned to the −OH groups on the nanoparticle surface. An intense peak is also found at 440 cm^{-1} assigned to the stretching of Zn−O bonds.[30] In the spectrum of neat PPS intense peaks can be observed at 1570 cm^{-1}, related to the symmetric stretching of the para-disubstituted aromatic rings, and at 1010 cm^{-1}, arising from the in-plane C−H bending;[14] the C=C stretching of the aromatic rings appears at 1470 cm^{-1} and the out-of-plane deformation vibration of =C−H takes place at 818 cm^{-1}. In addition, phenylene-sulfur stretching modes are found in the range of 1120−1030 cm^{-1}. New absorption peaks are found in the spectrum of the aminated derivative that corroborate the success of the amination reaction. The intense broad band centered at 3370 cm^{-1} is assigned to N−H stretching vibrations, the peak at 1620 cm^{-1} arises from N−H in-plane bending, and those at 830 and 770 cm^{-1} correspond to N−H out-of-plane bending modes (wagging and twisting).[31] The spectra of the nanocomposites show the characteristic peaks of both PPS-NH$_2$ and ZnO. The sample with 2.0 wt % loading exhibits a broadening and diminution in the intensity of the peak assigned to the N−H stretching vibrations, as well as a shift to lower wavenumber, by about 40 cm^{-1} in comparison to that of the modified polymer, indicative of the formation of hydrogen bonds between the amine groups of PPS-NH$_2$ and the hydroxyl groups of the nanoparticles. An analogous effect of band shift and widening has been observed in chitosan/ZnO[32] and poly(ester−amide) (PEA)/ZnO[30] nanocomposites, attributed to the existence of strong interactions between the −NH$_2$ of the matrix and the −OH groups on the ZnO surface. Moreover, the bands referred to the N−H bending modes are also shifted to lower wavenumbers; such result is also probably caused by the hydrogen bonding with the −OH groups of the nanoparticles. Further, the peak assigned to the stretching of Zn−O bonds is less intense and appears at 432 cm^{-1}, another indication of the strong nanoparticle−matrix interactions. Regarding the nanocomposite with 8.0 wt % loading, the shift and broadening of the bands related to N−H stretching and bending vibrations are considerably more pronounced. Most significantly, the N−H stretching appears at ~3300 cm^{-1}, thus corroborating the increased nanofiller−matrix interactions
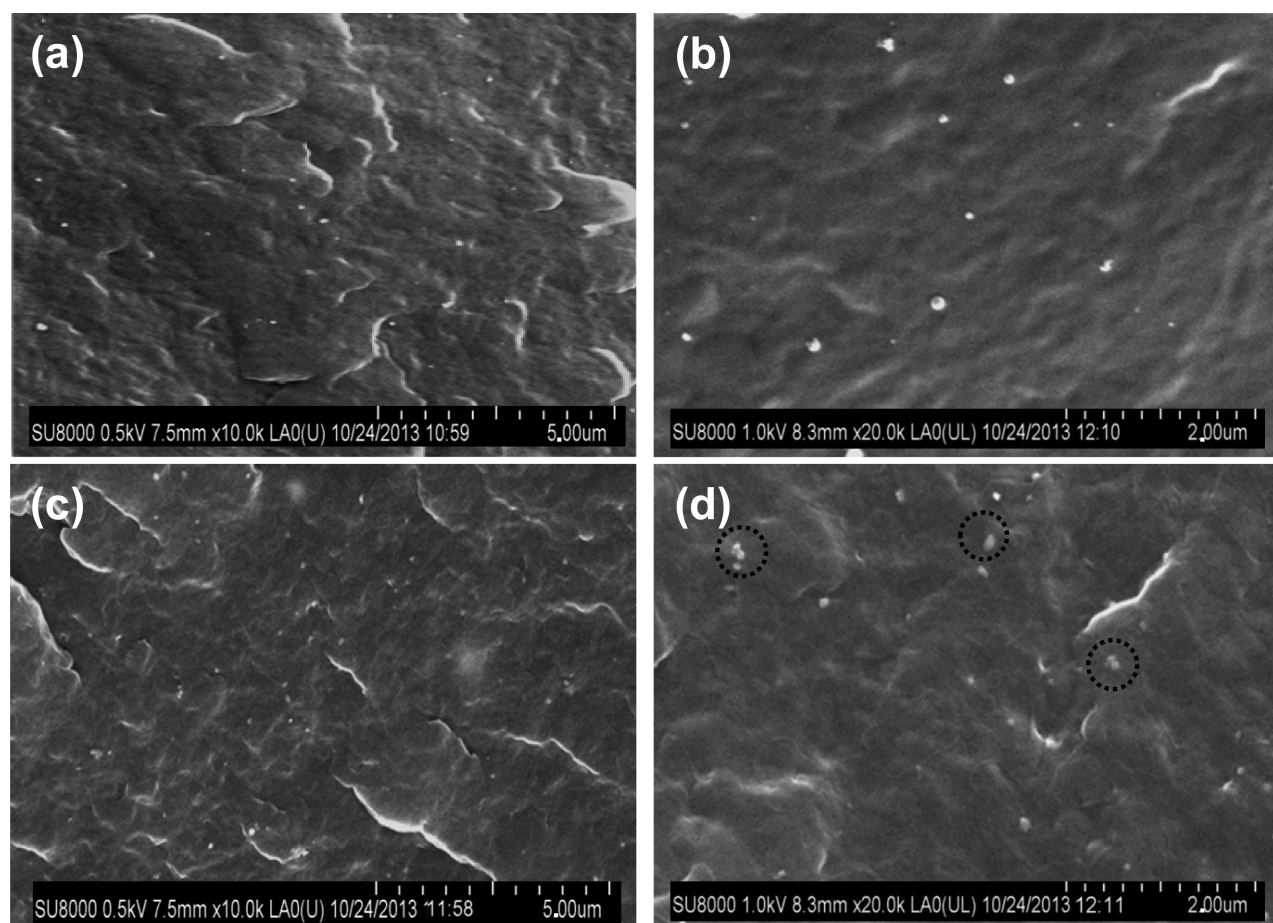
Figure 2. Typical SEM micrographs of PPS-NH$_2$/ZnO nanocomposites with (a, b) 2.0 wt % and (c, d) 8.0 wt % nanoparticle loading. The dashed circles in image d point to small clusters of 2 or 3 nanoparticles.
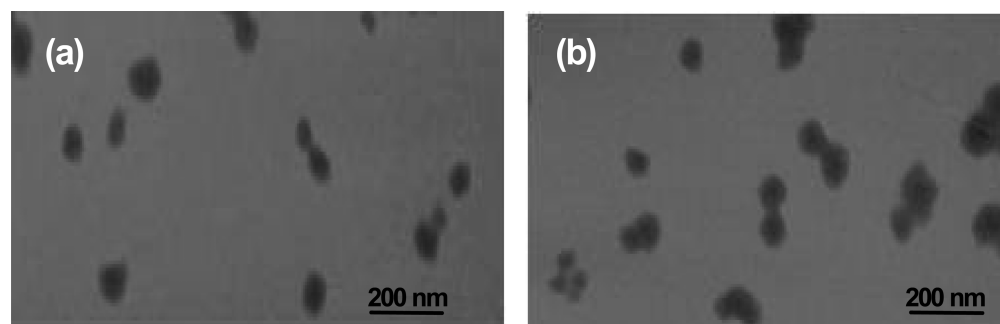
Figure 3. TEM images of PPS-NH$_2$/ZnO nanocomposites with (a) 4.0 wt % and (b) 8.0 wt % ZnO content.

upon rising nanofiller concentration. Besides, the peak related to Zn−O stretching shifts down to 425 cm^{-1} and displays increased intensity, in agreement with its higher ZnO content.

Morphological Analysis. The morphology of the nanocomposites was investigated by SEM, and typical images of PPS-NH$_2$ filled with 2.0 and 8.0 wt % ZnO are compared in Figure 2. The bright dots in the micrographs are the nanoparticles that display quasi-spherical shape, with a mean diameter of 75 nm. A random and uniform nanofiller dispersion can be observed in the nanocomposite with 2.0 wt % loading. Similar morphology was found for the nanocomposites incorporating 1.0 or 4.0 wt % ZnO, which suggests that the interactions between the −OH groups of the ZnO surface and the −NH$_2$ moieties of the polymer derivative prevent

nanoparticle aggregation. Further, the amination treatment should increase the hydrophilicity of the polymer,[33] improving the compatibility with the nanoparticles, thus promoting the interfacial adhesion between the two composite phases. As can be observed at higher magnification, the dispersion is finer in the nanocomposite with low ZnO content (Figure 2b), whereas that with 8.0 wt % loading presents not only well-dispersed nanoparticles but also a few small clusters composed of 2 or 3 particles (see the circles in Figure 2d). In contrast, for reference PPS/ZnO nanocomposites (see the Supporting Information, Figure S1), numerous large aggregates containing more than 6 particles were found at loadings ≥4.0 wt %, because of strong attractive forces among nanoparticles.

TEM analysis was also performed to assess the state of ZnO dispersion within the matrix, and typical micrographs of nanocomposites with 4.0 and 8.0 wt % loading are shown in Figure 3. In the sample with 4.0 wt % ZnO (Figure 3a), the nanoparticles are evenly and well distributed, without forming agglomerates. However, higher amounts of nanoparticles lead to increased propensity toward aggregation (Figure 3b), because the surface hydroxyl groups of ZnO have a strong tendency to create hydrogen bonds among nanoparticles due to the decrease in the interparticle distance, causing the formation of small clusters, in agreement with SEM observations. Overall, efficient nanoparticle dispersion within the modified polymer was attained without the need for coupling agents, making the manufacturing process of these nanocomposites simpler, shorter, and more economic.

Crystalline Structure. The influence of the nanoparticles on the crystalline morphology of the polymer derivative was studied by X-ray diffraction experiments, and the XRD patterns of ZnO nanoparticles, PPS, the modified polymer and nanocomposites with 2.0 and 8.0 wt % loading are shown in Figure 4. Neat PPS shows the most intense peak at $2\theta \approx 20.8°$,
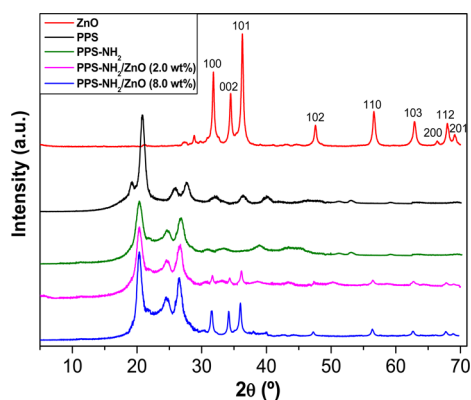

Figure 4. Room-temperature XRD patterns of ZnO, PPS, the aminated derivative, and PPS-NH$_2$/ZnO nanocomposites with 2.0 and 8.0 wt % ZnO.

arising from the overlap of the (111) and (200) reflections; peaks are also found at 19.2, 25.8, and 27.6°, assigned respectively to the (110), (112), and (211) crystalline planes of the orthorhombic unit cell.[14] The (110) crystalline reflection disappears in the diffractogram of PPS-NH$_2$, and the rest of the diffractions shift to lower 2θ values, indicating a change in the cell dimensions, albeit the orthorhombic structure is maintained. Further, the peaks are wider compared to those of the parent polymer, indicating a decrease in the crystallite size. The widening could also be related to the asymmetry induced by the random incorporation of the substituent groups.

On the other hand, ZnO nanoparticles exhibit characteristic peaks at 2θ values of 31.8, 34.4, 36.2, 47.6, 56.6, 62.9, 66.4, and 67.9°, arising from the diffraction of the (100), (002), (101), (102), (110), (103), (112), and (201) crystalline planes, respectively. All the Bragg reflections correspond to the hexagonal ZnO wurtzite structure.[21] These peaks, albeit less intense, can also be observed in the pattern of the nanocomposites, together with those characteristic of PPS-NH$_2$, hinting that the crystalline structure of both components is preserved. The level of crystallinity estimated from the diffractograms was 52, 48, 54, and 59% for PPS, PPS-NH$_2$ and its nanocomposites with 2.0 and 8.0 wt % loading, respectively,

pointing toward an increase in the overall crystallinity of the modified polymer upon addition of the nanoparticles. Moreover, the average crystallite sizes obtained from the (200), (112), and (211) planes of PPS were roughly estimated using the Scherrer equation[34] as 16, 18, and 20 nm, respectively, and dropped by an average of 18% for the polymer derivative. The nanocomposite with 2.0 wt % displays slightly higher crystallite size values than those of PPS-NH$_2$, whereas that with the highest nanoparticle content shows an average increment of 12%. This suggests that high amounts of ZnO effectively act as nucleating agents and favor the growth of the polymer crystals. Nevertheless, it should be noticed that the Scherrer formula gives only a lower bound of crystallite size because of several factors that influence on the width of the reflections, the most important being instrumental effects, inhomogeneous strain, and crystal lattice imperfections.[34]

Crystallization and Melting Behavior. It is well-known that the crystallization process plays a key role in the properties of polymer composites. The nonisothermal crystallization and melting behavior of PPS-NH$_2$ and the nanocomposites with different ZnO loading was investigated by means of DSC, and the corresponding thermograms are shown in Figure 5. The
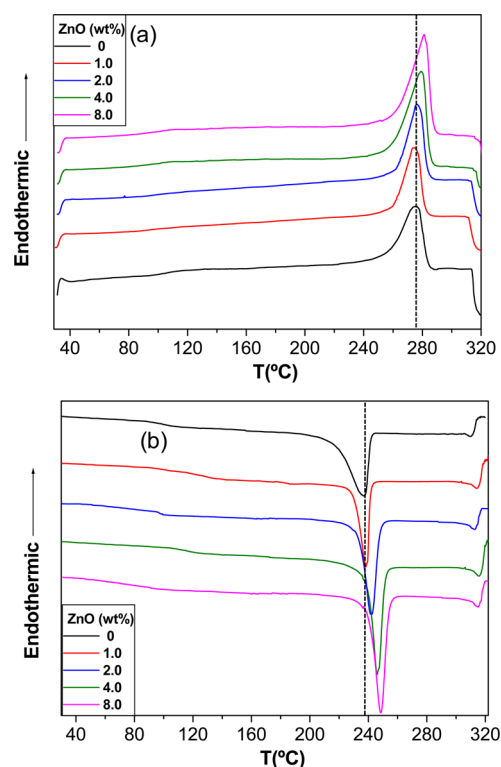
Figure 5. (a) DSC heating and (b) cooling thermograms of PPS-NH$_2$ and the nanocomposites with different ZnO loadings.

calorimetric parameters drawn from DSC curves of all the samples prepared in this work are collected in Table 1. The crystallization peak temperature (T_c) of PPS-NH$_2$ is 236 °C, about 10 °C lower than that of neat PPS, since the presence of the substituent groups reduces polymer chain motion, slowing down the crystallization process. Upon incorporation of ZnO, T_c gradually increases, by up to 13 °C at 8.0 wt % loading. Similar trends are found within the level of crystallinity (X_c) of the samples, which rises from 46% for the aminated derivative to almost 56% for the nanocomposite with the highest ZnO

Table 1. Thermal Parameters Obtained from DSC and TGA Analysis and Water Uptake for PPS-NH$_2$ and Its Nanocomposites Reinforced with ZnO Nanoparticles^a

material	T_c (°C)	T_m (°C)	X_c (%)	T_i (°C)	T_{10} (°C)	T_{max} (°C)	OI (%)	WU (%)
PPS-NH$_2$	236.2	274.9	46.3	377	445	509	33.2	0.029
PPS-NH$_2$/ZnO (1.0)	238.1	274.3	48.3	403	460	514	33.7	0.027
PPS-NH$_2$/ZnO (2.0)	242.2	276.4	52.5	408	478	523	34.3	0.025
PPS-NH$_2$/ZnO (4.0)	246.8	279.5	54.5	434	499	541	35.2	0.024
PPS-NH$_2$/ZnO (8.0)	249.3	281.0	55.7	449	507	549	37.2	0.021
PPS	246.1	279.2	52.5	458	501	540	31.7	0.026
PPS/ZnO (1.0)	248.1	280.3	53.4	462	513	543	32.1	0.023
PPS/ZnO (2.0)	249.6	280.4	53.8	464	516	545	32.5	0.022
PPS/ZnO (4.0)	246.5	278.6	50.1	456	507	539	33.3	0.025
PPS/ZnO (8.0)	243.2	277.9	48.7	447	496	530	34.8	0.028

^{a}For comparison, data of neat PPS and reference PPS/ZnO nanocomposites are also included. Values in parentheses indicate the ZnO content in wt %. T_m, peak melting temperature; T_c, peak crystallization temperature; X_c, degree of crystallinity; T_i, initial degradation temperature obtained at 2% weight loss; T_{10}, temperature for 10% weight loss; T_{max}, temperature of maximum rate of weight loss; OI, oxygen index parameter; WU, water uptake.

content. This indicates that the nanoparticles effectively act as heterogeneous nucleating agents for the matrix crystallization, promoting the crystal growth. Despite the strong interactions between PPS-NH$_2$ and ZnO could restrict the polymer chain mobility for crystallization, the good nanoparticle dispersion achieved in these nanocomposites leads to a very large number of nucleating centers, and the overall result is an increase in T_c and X_c. A different behavior is found for reference PPS based nanocomposites (Table 1), where both parameters increase slightly at low ZnO contents albeit decrease at concentrations ≥4.0 wt %. These facts suggest that when a small nanoparticle concentration is added to neat PPS, the nucleating effect predominates, while at higher concentrations the formation of large nanoparticle agglomerates hampers the polymer chain diffusion and crystal growth, leading to lower crystallinity and crystallization temperature. Therefore, the different crystallization behavior found for nanocomposites based on PPS or PPS-NH$_2$ seems to be directly related to the state of ZnO dispersion. It is important to note that PPS-NH$_2$/ZnO nanocomposites with nanoparticle loadings ≥4.0 wt % display higher crystallinity than the corresponding PPS/ZnO samples, which plays an important role on their mechanical performance, as will be discussed in a following section.

Regarding the melting temperature (T_m), the trends observed are similar to those discussed above for T_c, although the variations in comparison to the neat matrices are smaller (Table 1). Thus, this temperature increases gradually with the nanoparticle content, by about 6 °C for PPS-NH$_2$/ZnO (8.0 wt %) in relation to the value of the aminated polymer, while for reference PPS based nanocomposites rises up to a maximum value of 280 °C at 2.0 wt % loading and then decreases slightly. Overall, DSC results demonstrate the high nucleating capacity of well-dispersed ZnO nanoparticles.

Thermal and Moisture Resistance. Surgical precision instruments are subjected to high temperatures and moisture during pressurized steam sterilization processes in autoclave. Therefore, these materials require high heat resistance and very low moisture absorption in order to maintain their dimensional stability. To analyze the thermal stability of the nanocomposites, we carried out TGA characterization under a nitrogen atmosphere. The decomposition curves of ZnO, PPS, the aminated derivative, and the corresponding nanocomposites with different nanoparticle loadings are shown in Figure 6, and the characteristic degradation temperatures of all the
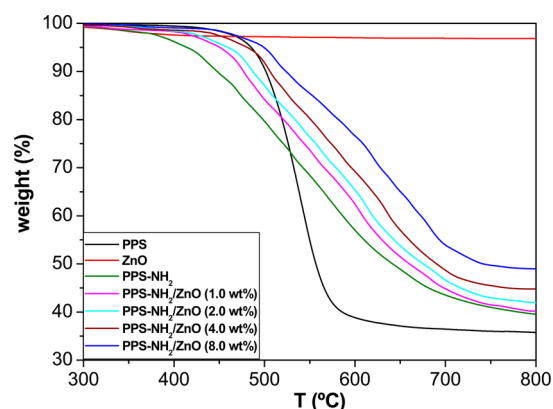
Figure 6. TGA curves under a nitrogen atmosphere for ZnO, PPS, the aminated derivative, and the nanocomposites with different ZnO contents.

samples are collected in Table 1. It can be observed that the bare nanoparticles display a very small weight loss (~0.8 wt %) below 300 °C, likely related to the removal of physically and chemically adsorbed water. Neat PPS exhibits a single degradation stage that initiates (T_i) at ~458 °C and shows the maximum rate of weight loss (T_{max}) around 540 °C (Table 1). A one step process is also observed for the aminated derivative, although it starts at a lower temperature than that of the parent polymer and occurs over a wider temperature range, indicating a lower degradation rate. Regarding PPS-NH$_2$/ZnO nanocomposites, the decomposition curve is similar to that of the matrix, albeit shifted to higher temperatures. A gradual raise in both T_i and T_{max} is found with increasing nanoparticle loading, the maximum increments being almost 80 and 40 °C, respectively, for the composite with 8.0 wt % ZnO. These unprecedented increases are ascribed to the presence of a ZnO network structure that strongly interacts with the matrix via H-bonding interactions and confines the motion of the polymer chains, and acts effectively as a mass transport barrier, hindering the migration of volatile products from the bulk of the matrix to the gas phase. Moreover, the high thermal conductivity of ZnO^{35} should facilitate heat dissipation within the composite, thus resulting in superior thermal stability. It is important to note that these exceptional thermal stability enhancements are considerably larger than those previously reported for PPS filled with other inorganic nanoparticles such as IF-WS$_2$ or Fe$_3$O$_4$[7] or
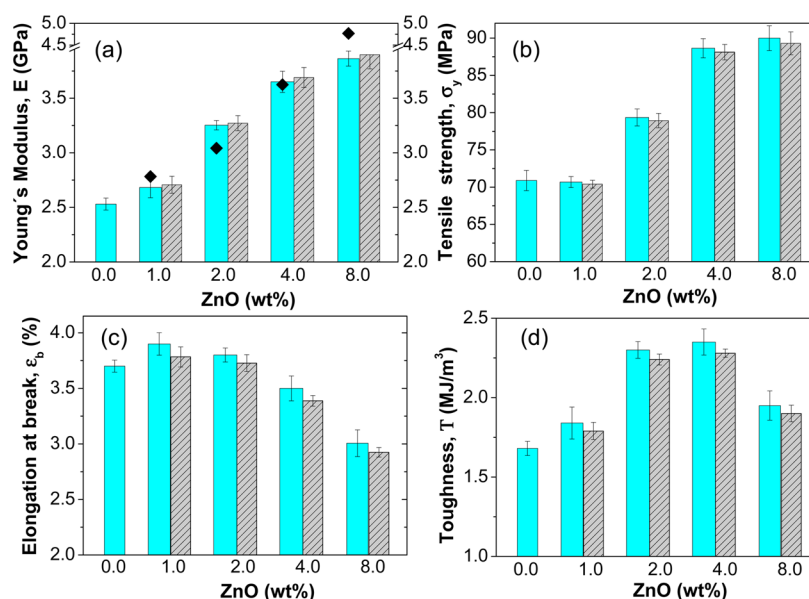
Figure 7. Comparison of the tensile properties of PPS-NH$_2$/ZnO nanocomposites with different nanoparticle loadings: (a) Young's modulus, (b) tensile strength, (c) strain at break, (d) toughness. The dashed bars correspond to samples subjected to 10 steam sterilization cycles. The solid symbols in a represent the theoretical values according to the rule of mixtures.

Table 2. Tensile and Thermomechanical Data for the Different Samples[a]

material	E (GPa)	σ_y (Mpa)	ε_b (%)	T (MJ/m^3)	T_g (°C)	$E'_{25°C}$ (GPa)	fwhm (°C)	tan δ_{area} (a.u.)	CTE (× 10^{-5}/°C)	HDT (°C)
PPS-NH$_2$	2.5	71.1	3.7	1.7	99.0	2.3	37.1	6.4	5.1	116.1
PPS-NH$_2$/ZnO (1.0)	2.7	70.3	3.9	1.8	97.5	2.6	39.5	6.8	4.6	114.3
PPS-NH$_2$/ZnO (2.0)	3.3	79.6	3.8	2.3	103.2	3.0	36.8	5.8	4.2	118.7
PPS-NH$_2$/ZnO (4.0)	3.7	88.2	3.5	2.4	109.7	3.3	38.3	5.9	3.9	123.5
PPS-NH$_2$/ZnO (8.0)	3.9	90.3	3.0	1.9	111.0	3.6	45.9	5.5	3.6	126.2
PPS	2.2	64.1	4.0	1.5	89.8	2.0	36.2	5.4	5.8	110.0
PPS/ZnO (1.0)	2.4	68.4	3.7	1.6	91.9	2.1	35.9	5.1	5.3	111.2
PPS/ZnO (2.0)	2.8	70.3	3.5	1.7	93.0	2.3	37.5	5.3	5.0	111.5
PPS/ZnO (4.0)	2.7	72.4	3.0	1.3	90.3	2.2	34.8	5.0	5.2	107.4
PPS/ZnO (8.0)	2.7	70.1	2.4	1.0	87.9	1.9	33.6	4.8	5.6	104.6

[a]E, Young's modulus; σ_y, tensile strength; ε_b, elongation at break; T, toughness; T_g, glass transition temperature; E', storage modulus; fwhm, full-width at half-maximum of tan δ peak; tan δ_{area}, area under tan δ peak; CTE, coefficient of linear thermal expansion; HDT, heat distortion temperature.

organic nanofillers like single-[36] or multiwalled carbon nanotubes.[37] However, a completely different behavior is found for reference PPS/ZnO nanocomposites (Table 1), where the degradation temperatures hardly increase or even decrease slightly at high nanoparticle contents due to weak PPS-ZnO interactions. This confirms the strong influence of the nanofiller−matrix interactions on the thermal properties of the nanocomposite.

It can also be observed from Figure 6 that the nanoparticles promote char residue formation. The weight of the residues under inert atmosphere can be correlated with the flame retardant ability of the nanocomposites through the oxygen index (OI),[21] which can be determined using Van Krevelen equation,[38] and the results are collected in Table 1. A material is regarded as flammable when its OI is lower than or equal to 26%. PPS has low flammability (OI ∼32%), and when burns it produces low amount of smoke and toxic gases. The aminated derivative shows a small increase in the OI value compared to that of the parent polymer, and it further rises slightly upon increasing ZnO content, resulting in an OI of 37.2% at 8.0 wt %. These increments should be associated with the high

thermal conductivity of ZnO, as discussed previously. The nanoparticles favor the rapid heat dissipation through the bulk of the composite, which means that it takes longer for the surface temperature of the sample to reach the ignition point. Overall, the results suggest higher fire resistance and reduced thermal aging upon addition of ZnO nanoparticles, which is interesting from an application viewpoint under different environments.

A MIS instrument must ensure water resistance during sterilization procedures. Therefore, the water uptake of the developed nanocomposites was tested, and the results are summarized in Table 1. PPS-NH$_2$ shows a low water uptake of ∼0.03%, which additionally decreases with increasing ZnO content, by about 27% at the highest nanoparticle loading. These results point out that the nanocomposites have improved barrier properties against water, which could be related to the more perfect crystalline structure of PPS-NH$_2$ matrix. Thus, the nanocomposites have reduced fraction of amorphous phase through which water molecules can permeate. Moreover, the higher degree of crystallinity increases the tortuosity of the transport path.[39] However, for reference PPS-based nano-

composites the water uptake increased upon addition of 8.0 wt % ZnO due to the reduction in the crystallinity of the polymer.

Static Mechanical Properties. In the field of medical technology, composites must comply with a high mechanical strength, modulus, and impact resistance. Therefore, it is of great interest to investigate the static mechanical properties of PPS-NH$_2$/ZnO nanocomposites by means of tensile tests. Their average Young's modulus (E), tensile strength (σ_y), elongation at break (ε_b), and toughness (T) values are compared in Figure 7. Tensile data for all the samples tested are collected in Table 2. The aminated polymer exhibits a Youngs modulus of about 2.5 GPa (Figure 7a), slightly higher than that of PPS. The incorporation of the ZnO imparts the high stiffness of the fillers to the matrix, leading to a remarkable E enhancement, by up to 55% at 8.0 wt %. Very similar trend is found for the tensile strength (Figure 7b). These improvements are associated with the strong ZnO-matrix interactions via H-bonding, fact that promotes the adhesion between the two phases, resulting in improved load transfer. Moreover, they are likely related to the increase in crystallinity (Table 1), because enhanced secondary interchain bonding results from adjacent chain segments when the molecular chains are closely packed and parallel, thereby inhibiting relative interchain motion. In contrast, smaller stiffness and strength improvements are found for the reference composites based on a PPS matrix (Table 2), where E shows a maximum augment of 27% at 2.0 wt % ZnO and decreases at higher loadings due to weak filler−matrix adhesion, poor nanoparticle dispersion, and the drop in the matrix crystallinity. The behavior found for ZnO-reinforced PPS or PPS-NH$_2$ nanocomposites differs from that reported for similar nanocomposites incorporating small amounts of other nanoparticles such as Al$_2$O$_3$,[40] TiO$_2$, or CuO,[28] where the mechanical strength of PPS decreased because of a weakening of the matrix induced by the presence of a heterogeneous phase.

Taking into account the reported Young's modulus for ZnO,[41] the theoretical E values for PPS-NH$_2$-based nanocomposites were estimated by the rule of mixtures (see solid symbols in Figure 7a). Experimental Young's modulus values were in good agreement with the theoretical calculations (differences <7%) except for that with the highest ZnO loading, where the calculated value was about 20% higher than the experimental one. As mentioned above, the increase in modulus attained in these nanocomposites arises from the increase in the matrix crystallinity, not only from direct reinforcement effect. The model considers that the moduli of the composite phases are independent; however, the nanoparticles promote the crystallization of the polymer close to their surfaces, thus influencing the matrix. Thus, the properties of the interfacial matrix probably differ from those of the bulk matrix, and this might explain the discrepancies between the theoretical and experimental data, particularly in the nanocomposite with 8.0 wt % ZnO that shows the maximum level of crystallinity.

Regarding the elongation at break (Figure 7c), no significant change is observed for PPS-NH$_2$ nanocomposites up to 4.0 wt % nanoparticle content, showing a small decrease at higher loadings. In contrast, ε_b systematically drops for reference PPS-based nanocomposites (Table 2), by up to 40% at 8.0 wt % loading in comparison to that of the pure polymer, because of the presence of big aggregates that obstruct the ductile flow of the polymer chains. Another important parameter is the area under the tensile curve, which is a measure of the toughness of the system (Figure 7d). In the case of PPS-NH$_2$/ZnO

nanocomposites, this area is larger than that of the aminated polymer, showing a maximum increment of 42% at 4.0 wt % ZnO. However, for the reference PPS/ZnO composites, the toughness is roughly maintained up to 2.0 wt % and then falls moderately (Table 2), showing a drop of around 33% at the highest loading. These results indicate that composites with the aminated derivative exhibit improved capability to absorb energy during deformation, arising from an enhanced matrix-nanoparticle interfacial adhesion, hence a more effective barrier against crack propagation.

To evaluate the effects of sterilization on the mechanical properties of the composites, we carried out tensile tests on samples subjected to 10 steam sterilization cycles, and the results are also shown in Figure 7. The comparison between data obtained before and after sterilization reveals that the Youngs modulus and tensile strength of all the nanocomposites remain unchanged (differences lower than 1%), whereas the elongation at break and toughness exhibit a small drop (≤3%), albeit the changes are insignificant. The results indicate that the autoclave sterilization process does not alter the tensile properties of these nanomaterials.

Thermomechanical Properties. The influence of ZnO nanoparticles on the dynamic mechanical properties of the composites was evaluated by DMA. Figure 8 presents the
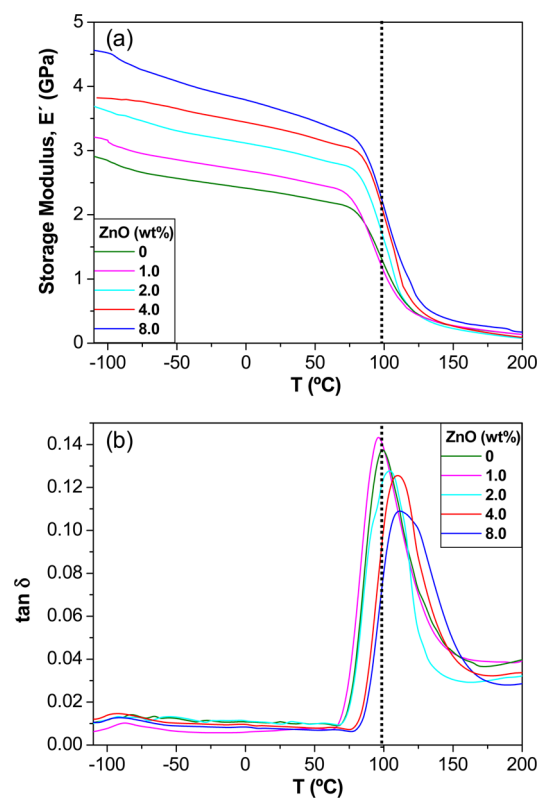
Figure 8. (a) Storage modulus E' and (b) tan δ as a function of temperature for the aminated polymer and its nanocomposites with different contents of ZnO nanoparticles.

evolution of the storage modulus (E') and loss factor (tan δ) vs temperature for PPS-NH$_2$ and the nanocomposites with different ZnO concentrations at the frequency of 1 Hz. The dynamic mechanical spectra for reference PPS/ZnO nanocomposites were also recorded, and their T_g and E' values at 25 °C are collected in Table 2. Regarding PPS-NH$_2$/ZnO

nanocomposites, E′ increases progressively with the addition of the nanoparticles at temperatures below the glass transition (Figure 8a), up to 56% at 8.0 wt % ZnO. In contrast, only small increases and even some decrements in the matrix modulus are found for reference PPS based composites (Table 2), being the highest increment of 15% at 2.0 wt % loading. The improved behavior found for the composites with the aminated polymer as compared to those based on pure PPS should be related to their stronger filler−matrix interfacial adhesion combined with their higher crystallinity and improved nanoparticle dispersion, as discussed previously.

The evolution of the tan δ (ratio of the loss to storage modulus, Figure 8b) as a function of temperature exhibits an intense peak whose maximum corresponds to the T_g. The aminated derivative shows a T_g value close to 100 °C (Table 2), about 10 °C higher than that of neat PPS, ascribed to the restrictions on the mobility of the polymer chains in the amorphous region imposed by the intermolecular interactions between polar groups. Reference PPS based nanocomposites only show small rises in this transition temperature compared to that of neat PPS, while PPS-NH$_2$/ZnO samples show a gradual rise upon increasing nanoparticle concentration, of up to 12 °C at the highest loading tested. This remarkable increment should be ascribed to the interaction between the amine groups of the modified polymer and the hydroxyl groups of the ZnO surface via hydrogen bonding, combined with the good nanoparticle dispersion that results in large matrix−filler interfacial contact area. As a consequence, the polymer chains are effectively immobilized, resulting in a strong T_g enhancement, higher than that found upon incorporation of similar amount of other inorganic nanoparticles such as quasi-spherical WS$_2$.[7] Moreover, a broadening of the tan δ peak is found upon addition of the ZnO, particularly for the nanocomposite with 8.0 wt % content (Table 2), which shows a full-width at half-maximum (fwhm) value around 9 °C higher than that of PPS-NH$_2$. This result might originate from a less homogeneous amorphous phase in the nanocomposites compared to that of the aminated polymer, and has also been explained in terms of a larger volume of the interface.[42] Thus, a raise in the nanoparticle concentration should lead to increased nanoparticle−matrix interactions via hydrogen bonding and larger interfacial area, and the molecular motions at the interface region also contribute to the damping of the material.[43] Therefore, the behavior observed suggests that there are molecular relaxations in the nanocomposites that are not present in the aminated polymer. The broadening can also be explained in terms of the difference between the physical state of the matrix surrounding the nanoparticles (a shell of immobilized polymer layer) compared to the bulk matrix. On the contrary, the tan δ peak of reference PPS composites is similar or even narrower than that of the pure polymer, suggesting weaker nanofiller−matrix adhesion.

Further, the incorporation of the nanoparticles in PPS-NH$_2$ matrix reduces the height of the tan δ peak by restricting the movement of the polymer chains. The magnitude of the tan peak δ is related to the nature of the polymer system.[43] In an unfilled polymer, the chain segments are free from constraints. The introduction of the nanoparticles causes a reduction in chain mobility, thus reducing the peak height. Moreover, a high value of tan δ typically indicates imperfections in the elasticity of a system. Therefore, the lower tan δ in the nanocomposites suggests that when the stress is eliminated, the energy stored

during the deforming process is recuperated more rapidly in comparison to the neat polymer.

It is also interesting to analyze the influence of ZnO on the area under the tan δ peak (Table 2), given that this area is indicative of the energy dissipated in the viscoelastic relaxations.[44] PPS-NH$_2$ based nanocomposites containing low ZnO contents display comparable area than that of the aminated polymer, confirming that low amounts of nanoparticles improve the matrix stiffness without a detriment in its ability to dissipate energy. However, a small drop is found for the sample with the highest loading, probably related to the increased nanoparticle−matrix interactions. In contrast, for the reference PPS/ZnO composites this area is progressively reduced with increasing nanoparticle concentration, indicating a diminution in the material ability to dissipate energy.

The heat distortion temperature (HDT) is an indication of the dimensional stability of a material under a specific load and temperature, and is an important parameter that has to been taken into account during the product design step. Several factors affect the HDT of polymer materials, namely the stiffness, the level of crystallinity and the T_g. The inclusion of nanofillers such as carbon nanotubes[45] or WS$_2$ nanoparticles[29] has been reported to increase the HDT of PPS. Table 2 summarizes the HDT data for all the samples studied in this work. The addition of ZnO to PPS-NH$_2$ leads to a raise in this parameter, by up to 10 °C at 8.0 wt % loading. This noticeable increment originates from the concurrent increase in the three parameters influencing the HDT. In contrast, a small drop is found upon incorporation of ZnO contents ≥4.0 wt % to neat PPS, which likely arises from the reduction in crystallinity found for those composites (Table 1) combined with a slight decrease in T_g and a small reinforcement effect (Table 2).

Another important thermomechanical property used in the design of nanocomposites for precision surgical instruments/devices is the coefficient of thermal expansion (CTE). A low CTE is desirable to preserve the dimensional stability of the material, and can be achieved by dispersing hard nanoparticles with low CTE within the matrix.[45] Table 2 collects the CTE data at 25 °C for the different composites. The CTE of PPS-NH$_2$ is ~5.1 × 10^{-5}/°C, slightly lower than that of the parent polymer, and drops steadily upon addition of increasing ZnO loadings, by nearly 30% for the nanocomposite with the highest nanoparticle concentration. This remarkable fall should be related to the improvement in the matrix stiffness due to the presence of the nanoparticles that obstruct the thermally induced movements of the polymeric chains, combined with their strong interaction with the matrix that provide a high level of motion restriction. Moreover, ZnO displays significantly lower CTE than the matrix,[46] fact that contributes to the reduction in this property. In contrast, the CTE of pure PPS increases slightly upon incorporation of ZnO loadings ≥4.0 wt % (Table 2), because the nanoparticles are weakly adhered to the polymer; further, they are agglomerated in certain regions of the matrix, leaving the others free from motion constrains.

Tribological Properties. With a view to use these nanocomposites in high-performance medical instruments like MIS products, it is crucial to investigate their tribological properties. Hard inorganic nanoparticles generally improve the tribological performance of polymers, and their efficiency is determined by a number of factors like the nanocomposite microstructure, filler size and shape, state of nanoparticle dispersion, and quality of the filler−matrix interface.[47] Figure 9a compares the mean coefficient of friction (μ) for PPS-NH$_2$ and

10140

dx.doi.org/10.1021/am501610p | ACS Appl. Mater. Interfaces 2014, 6, 10132−10145
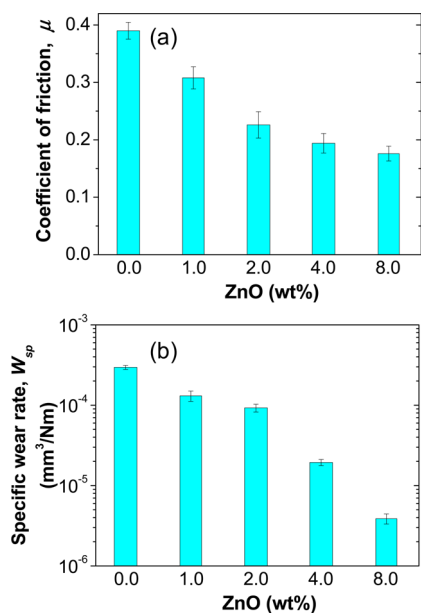
Figure 9. Tribological properties of PPS-NH$_2$/ZnO nanocomposites: (a) coefficient of friction and (b) specific wear rate.

the corresponding nanocomposites. The value of μ for the aminated derivative is about 0.38, similar to that of the parent polymer, and decreases steadily upon addition of ZnO, by up 52% at the highest nanoparticle content. This behavior is ascribed to the superior stiffness, strength and toughness of the composites, as revealed by tensile tests. Thus, the ZnO nanoparticles can restrain the scuffing and adhesion of the matrix during sliding, leading to higher resistance against the penetration of the hard asperities on the countersurface than the neat polymer, which combined with the increase in heat conductivity, hence lower temperature in the sliding contact, leads to lower μ values. This behavior differs to that found for reference PPS/ZnO nanocomposites (see the Supporting Information, Figure S2), where μ increased upon increasing nanoparticle loading, probably related to their poorer mechanical performance. Thus, Yu et al.[48] compared the

friction coefficient of neat PPS and composites incorporating dry lubricants such as graphite, MoS$_2$ and PTFE, and reported that PPS/graphite composite showed the lowest μ, ascribed to its superior mechanical performance. Analogous trend is observed in the present study, where the lowest μ is found for the nanocomposite with the highest stiffness and strength.

Regarding the specific wear rate (W_{sp}), a very strong reduction is found upon addition of the nanoparticles compared to that of the aminated derivative ($\sim 3 \times 10^{-3}$ mm^3/Nm, Figure 9b). In particular, the nanocomposite with the highest loading shows nearly 100-fold decrease in this property. This unprecedented enhancement in wear resistance is ascribed to the improved mechanical properties of this nanocomposite and the strong filler−matrix interfacial adhesion via H-bonding, facts that typically result in the development of a thin and uniform transfer film, hence enhanced tribological properties. Chang and Zhang,[49] dealing with nano-TiO$_2$ reinforced composites, suggested a rolling mechanism in which the nanoparticles rolled between the surfaces rather than slide, and consequently decreased the shear stress, contact temperature and coefficient of friction. Schwartz and Bahadur,[40] working with PPS/Al$_2$O$_3$ nanocomposites, proposed that the nanoparticles could be readily transferred to the countersurface, and would remain embedded in the transfer film, providing strong anchoring to the asperities of the countersurface, thereby increasing the bonding strength between the transfer film and the steel surface. Such mechanisms could be a suitable explanation for the improvements in μ and W_{sp} observed in this work. This behavior is in contrast to that reported by Bahadur and Sunkara[28] for PPS/ZnO nanocomposites, where the incorporation of the nanoparticles provoked an increase in both μ and W_{sp}, attributed to poor nanoparticle dispersion and the formation of a discontinuous and poorly bonded transfer film. Further, the flexural strength of these nanocomposites was lower than that of the neat polymer, due to weak nanofiller−matrix interfacial adhesion. It is also worth noting that PPS-NH$_2$/ZnO nanocomposites possess considerably improved tribological properties compared with similar composites reinforced with other inorganic nanoparticles such as Al$_2$O$_3$, TiO$_2$, CuO and SiC[28,40] and slightly better than those reported for hybrids incorporating WS$_2$.[50] The comparison of the results
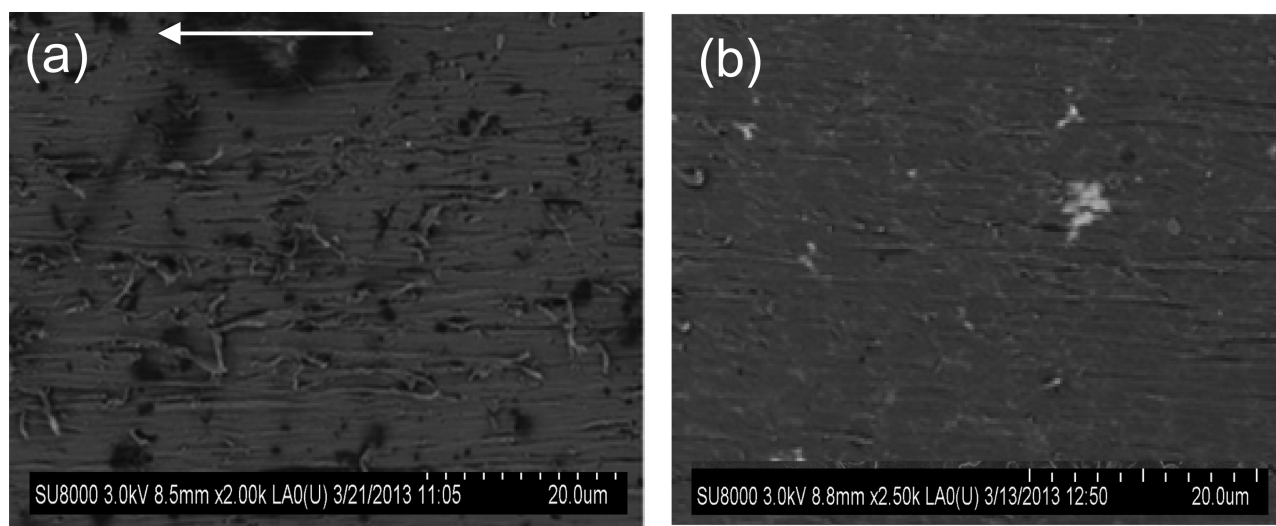
Figure 10. SEM micrographs of the worn surfaces of: (a) PPS-NH$_2$ and (b) PPS-NH$_2$/ZnO nanocomposite with 8.0 wt % loading. The arrow indicates the sliding direction.

obtained from the different studies demonstrates the strong influence of the filler−matrix interfacial adhesion on the tribological performance.

Figure 10 compares SEM images of the worn surfaces of the aminated derivative and the corresponding nanocomposite with the highest ZnO loading. Stretches, deep grooves, fractures and some scuffing can be observed on the worn surface of PPS-NH$_2$ (Figure 10a). The surface also reveals a plastic flow and ribbon-like chips that might be caused by microploughing sliding action, suggesting that adhesive wear is the dominant mechanism under sliding conditions. In contrast, the nanocomposite exhibits a smoother surface (Figure 10b), without marks of scuffing or cracking. Further, the grooves on the worn surface are shallower and the degree of plastic deformation is reduced. The addition of nanoparticles minimizes the adhesive wear and increases the surface hardness, resulting in improved tribological performance.

Dielectric Properties. MIS instruments require superior dielectric properties, since they should provide insulation characteristics when used in electrosurgical procedures. The choice of dielectric material is very important in applications where elevated voltages are expected, for instance, in the case of a forceps, to insulate the handle assembly from high voltage during electrocautery. A good insulating material should have both low dielectric constant (ε') and dielectric loss (ε''). The dielectric properties of materials are primarily conditioned by their polarizabilities at a given frequency. For composite systems, when free charge carriers move through the material, charges accumulate at the matrix−filler interface due to the mismatch of the conductivities and dielectric constants of the components. This effect is known as interfacial polarization,[51] and can be identified in the frequency region between 1×10^2 and 1×10^5 Hz. The changes in dielectric properties as a function of frequency are attributed to dielectric relaxations, and are more significant at low frequencies because of the Brownian motion of the chain segments.[51]

Figure 11 shows the evolution of ε' and ε'' vs frequency for PPS-NH$_2$ and the corresponding nanocomposites. Both parameters decrease with increasing frequency, which could be ascribed to the tendency of dipoles in polymeric samples to orient themselves in the direction of the applied field. However, at frequencies $>10^4$ Hz the dielectric properties remain almost constant, likely related to the orientation of the dipoles, which difficult the rotation at high frequency. The addition of polar ZnO to PPS-NH$_2$ causes an increase in the dielectric constant (Figure 11a), particularly at low frequencies (i.e., $<1 \times 10^3$ Hz). Similar phenomenon has been observed in polyurethane (PU)/ZnO nanocomposites,[52] attributed to the large permittivity of ZnO which enhances the polarization via dipole−dipole interactions among neighbor nanoparticles. For instance, at 1×10^2 Hz, the increments in ε' in comparison to the value of the matrix are 2, 7, 14 and 22% for ZnO loadings of 1.0, 2.0, 4.0, and 8.0 wt %, respectively. Nevertheless, for all the samples, ε' remains below 4 in the whole frequency region studied; hence PPS-NH$_2$/ZnO nanocomposites possess a dielectric constant low enough to be used as insulating materials in medical devices.[53] A qualitatively similar increasing trend is found for ε'' (Figure 11b), albeit in all cases this parameter is lower than 1×10^{-3} in the range of 1×10 to 1×10^6 Hz, which indicates very low energy dissipated in the form of heat. Overall, results demonstrate that the developed nanocomposites can be effectively used as dielectric materials.
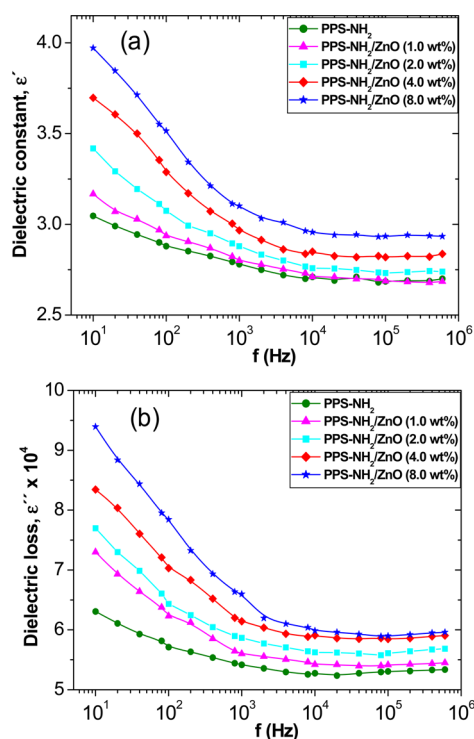
Figure 11. Frequency dependence of (a) the dielectric constant and (b) dielectric loss for PPS-NH$_2$/ZnO nanocomposites.

Antibacterial Activity. The antibacterial activity of PPS-NH$_2$ and the nanocomposites was examined against two human pathogen bacteria: *E. coli* (Gram-negative) and *S. aureus* (Gram-positive), and the results are shown in Figure 12. It
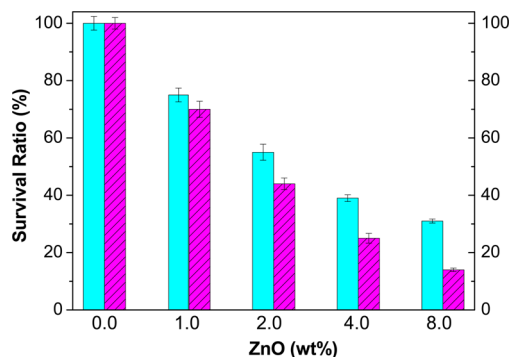
Figure 12. Antibacterial properties of PPS-NH$_2$-based composites with different ZnO loadings against *S. aureus* (solid bars) and *E. coli* (dashed bars).

can be observed that the survival ratio of both bacteria drops with increasing nanoparticle concentration, the decrease being more pronounced at low loadings, and the best antibacterial action (about 69 and 86% growth inhibition against *S. aureus* and *E. coli*, respectively) was obtained at 8.0 wt % ZnO. For the same nanoparticle content, these composites exhibit significantly lower survival ratio, and consequently better antibacterial properties, than the reference PPS/ZnO nanocomposites (see the Supporting Information, Figure S3), which can be explained in terms of their improved filler dispersion, hence larger effective surface area. This demonstrates that the nanofiller concentration and state of dispersion are two key factors affecting the antibacterial properties. Interestingly, all the

nanocomposites display stronger antibacterial effect on *E. coli* than on *S. aureus*. This is in agreement with previous studies on ZnO-reinforced polymer composites[22] that found a more effective antibacterial activity against Gram-negative bacteria, and that high ZnO loading in the composites can significantly inhibit the growth of the microorganisms. The different behavior against these two bacteria is probably ascribed to differences in the structure and chemical composition of their surfaces (cell wall and membranes).[54]

Concerning the antibacterial activity of ZnO nanoparticles, various mechanisms have been proposed:[54,55] the release of Zn^{2+} ions, the mechanical damage of the cell membranes due to the incursion of the nanoparticles, and the production of H_2O_2 from the nanoparticle surface. Tam and co-workers[56] investigated the antibacterial activity of ZnO (~10 nm diameter) against Gram-positive and Gram-negative bacteria and found very few cases of cellular internalization of the nanoparticles. In the present work, the nanoparticles possess an average diameter of 75 nm, consequently they are not expected to penetrate through the cell wall to damage the bacteria. On the other hand, ZnO is in general unstable in solution,[56] and the Zn^{2+} concentration increases as a result of ZnO decomposition; therefore, the release of Zn^{2+} is a possible reason for the biocide action. These nanocomposites display antimicrobial action in the absence of UV light, in agreement with previous studies[19,56] that explored the antibacterial activity of nano-ZnO without irradiation and demonstrated that it was related to the release of H_2O_2 from the ZnO. Therefore, the production of H_2O_2 (a powerful oxidizing agent harmful to the cells of microorganisms) from the ZnO surface can be regarded as the main factor of antibacterial activity of ZnO-reinforced nanocomposites, and the different action toward *E. coli* and *S. aureus* is likely caused by the different sensitivities toward the H_2O_2 generated. Overall, results reveal the great potential of the developed nanocomposites to induce antibacterial property, which is interesting for biomedical applications.

4. CONCLUSIONS

The morphology, thermal, mechanical, tribological, dielectric, and antibacterial properties of an aminated PPS derivative incorporating different loadings of ZnO nanoparticles have been studied. The nanocomposites were manufactured by conventional melt-blending and compression molding without the need for coupling agents. SEM and TEM analyses revealed a good distribution of the nanoparticles within the matrix, showing finer dispersion for samples with lower ZnO contents. FT-IR spectra demonstrated the existence of strong ZnO-matrix interactions via hydrogen bonding. DSC thermograms showed that the nanoparticles act as heterogeneous nucleating agents for PPS-NH$_2$, raising its crystallization temperature and level of crystallinity, whereas no change in its crystalline structure was detected. TGA experiments indicated a strong rise in the thermal stability of the matrix upon increasing ZnO concentration, by up to 80 °C in the initial degradation temperature at 8.0 wt % ZnO. A noteworthy increase in the storage modulus and glass transition temperature was also observed, as revealed by DMA. In addition, the stiffness, strength, toughness and heat distortion temperature significantly improved, demonstrating the noticeable reinforcing effect of these nanoparticles. Further, tensile properties remained nearly unchanged after several cycles of steam sterilization in autoclave. A reduction in the CTE was also observed, because the strong nanofiller−matrix interactions

hinder the thermally induced movements of the polymeric chains. More importantly, a significant decrease in the coefficient of friction and an unprecedented drop in the wear rate of almost 100-fold were found. The dielectric constant and dielectric loss increased with ZnO concentration, albeit they remained low enough to fulfill the requirements for insulating materials used in electrosurgical applications. The nanocomposites showed active inhibition against human pathogenic bacteria, and the percentage of inhibition increased with the nanoparticle content. These lightweight high-performance nanocomposites show lower water absorption and considerably improved heat resistance, mechanical, tribological and antibacterial properties compared to those of PPS/ZnO, and are useful for medical applications in which high demands are imposed on the material in terms of its dimensional stability, stiffness, strength, temperature/moisture resistance, damage/wear resistance, dielectric properties and resistance to repeated sterilization. In particular, they are suitable for the development of minimally invasive surgical instruments such as scissors, forceps, clamps, microgrips and hooks used in different disciplines like vascular, cardiac or thoracic surgery, urological and gynecological procedures. They can also be used in ventilator respiratory gas blocks, instruments for diagnostic purposes such as endoscopes and other specialized medical tubing applications. In addition, these nanomaterials are appropriate in dental applications for tartar and plaque removal devices as well as hand-held tools for dispensing a pasty filling material.

■ ASSOCIATED CONTENT

Ⓢ Supporting Information
Morphology, tribological, and antibacterial properties of reference PPS/ZnO nanocomposites. This material is available free of charge via the Internet at http://pubs.acs.org/

■ AUTHOR INFORMATION

Corresponding Author
*E-mail: adiez@ictp.csic.es.
Notes
The authors declare no competing financial interest.

■ ACKNOWLEDGMENTS

■ REFERENCES

(1) Sanchez, C.; Belleville, P.; Polpall, M.; Nicole, L. Applications of Advanced Hybrid Organic-Inorganic Nanomaterials: from Laboratory to Market. *Chem. Soc. Rev.* **2011**, *40*, 696−753.

(2) Rozenberg, B. A.; Tenne, R. Polymer-assisted Fabrication of Nanoparticles and Nanocomposites. *Prog. Polym. Sci.* **2008**, *33*, 40−112.

(3) Kickelbick, G. Concepts for the Incorporation of Inorganic Building Blocks into Organic Polymers on a Nanoscale. *Prog. Polym. Sci.* **2003**, *28*, 83−114.

(4) Zou, H.; Wu, S.; Shen, J. Polymer/Silica Nanocomposites: Preparation, Characterization, Properties, and Applications. *Chem. Rev.* **2008**, *108*, 3893−3957.

(5) Caseri, W. Inorganic Nanoparticles as Optically Effective Additives for Polymers. *Chem. Eng. Commun.* **2009**, *196*, 549−572.

(6) Jeon, I. Y.; Baek, J. B. Nanocomposites Derived from Polymers and Inorganic Nanoparticles. *Materials* **2010**, *3*, 3654−3674.

(7) Naffakh, M.; Diez-Pascual, A. M.; Marco, C.; Ellis, G. J.; Gomez-Fatou, M. A. Opportunities and Challenges in the Use of Inorganic Fullerene-like Nanoparticles to Produce Advanced Polymer Nanocomposites. *Prog. Polym. Sci.* **2013**, *38*, 1163−1231.

(8) Tiwari, A. *Recent Developments in Bio-Nanocomposites for Biomedical Applications*; Nova Science Publishers: New York, 2010.

(9) Fernandes, R.; Gracias, D. H. Toward a Miniaturized Mechanical Surgeon. *Mater. Today* **2009**, *12*, 14−20.

(10) Darzi, S. A.; Munz, Y. The Impact of Minimally Invasive Surgical Techniques. *Annu. Rev. Med.* **2004**, *55*, 223−237.

(11) Sastry, V. R. *Plastics in Medical Devices: Properties, Requirements and Applications*; Elsevier: Burlington, MA, 2010.

(12) Wang, W.; Zhu, Y.; Liao, S.; Li, J. Carbon Nanotubes Reinforced Composites for Biomedical Applications. *Biomed. Res. Inter.* **2014**, *2014*, 518609−518623.

(13) Wayne, H.; Hill, H. W.; Brady, D. G. In *Encyclopedia of Polymer Science and Engineering*, 2nd ed.; Mark, H. F., Bikales, N., Overberger, C. C., Menges, G., Kroschwitz, J., Eds.; Wiley-Interscience: New York, 1988; Vol *11*, p 531.

(14) Diez-Pascual, A. M.; Naffakh, M. Synthesis and Characterization of Nitrated and Aminated Poly(phenylene sulfide) Derivatives for Advanced Applications. *Mater. Chem. Phys.* **2012**, *131*, 605−614.

(15) Diez-Pascual, A. M.; Naffakh, M. Grafting of an Aminated Poly(phenylene sulphide) Derivative to Functionalized Single-walled Carbon Nanotubes. *Carbon* **2012**, *50*, 857−868.

(16) Diez-Pascual, A. M.; Naffakh, M. Towards the Development of Poly(phenylene sulphide) Based Nanocomposites with Enhanced Mechanical, Electrical and Tribological properties. *Mater. Chem. Phys.* **2012**, *135*, 348−357.

(17) Jeon, I.-Y.; Lee, H.-J.; Choi, Y. S.; Tan, L.-S.; Baek, J.-B. Semimetallic Transport in Nanocomposites Derived from Grafting of Linear and Hyperbranched Poly(phenylene sulfide)s onto the Surface of Functionalized Multi-Walled Carbon Nanotubes. *Macromolecules* **2008**, *41*, 7423−7432.

(18) Schmidt-Mende, L.; Macmanus-Driscoll, J. L. ZnO − Nanostructures, Defects, and Devices. *Mater. Today* **2007**, *10*, 40−48.

(19) Yamamoto, O. Influence of Particle Size on the Antibacterial Activity of Zinc Oxide. *Int. J. Inorg. Mater.* **2001**, *3*, 643−646.

(20) Subramani, C.; Mhaske, S. T.; Kathe, A. A.; Varadarajan, P. V.; Virendra, P.; Nadanathangam, V. Functional Behavior of Polypropylene/ZnO-Soluble Starch Nanocomposites. *Nanotechnology* **2007**, *18*, 385702−385710.

(21) Diez-Pascual, A. M.; Diez-Vicente, A. L. Development of Nanocomposites Reinforced with Carboxylated Poly(ether ether ketone) Grafted to Zinc Oxide with Superior Antibacterial Properties. *ACS Appl. Mater. Interfaces* **2014**, *6*, 3729−3741.

(22) Chang, B. P.; Akil, H. M.; Nasir, R. M.; Nurdijati, S. Abrasive Wear Performance and Antibacterial Assessment of Untreated and Treated ZnO-reinforced Polymer Composite. *Polym. Compos.* **2013**, *34*, 1020−1032.

(23) Wang, Y.; Shi, J.; Han, L.; Xiang, F. Crystallization and Mechanical Properties of T-ZnOw/HDPE Composites. *Mater. Sci. Eng., A* **2009**, *501*, 220−228.

(24) Shi, J.; Wang, Y.; Gao, Y.; Bai, H. Effects of Coupling Agents on the Impact Fracture Behaviors of T-ZnOw/PA6 Composites. *Compos. Sci. Technol.* **2008**, *68*, 1338−1347.

(25) Li, F.; Hu, L.; Li, Z.; Huang, X. Influence of Temperature on the Morphology and Luminescence of ZnO Micro and Nanostructures Prepared by CTAB-Assisted Hydrothermal Method. *J. Alloys Compd.* **2008**, *465*, L14−L19.

(26) Rataboul, F.; Nayral, C.; Casanove, M. J.; Maisonnat, A.; Chaudret, B. Synthesis and Characterization of Monodisperse Zinc and Zinc Oxide Nanoparticles from the Organometallic Precursor [Zn(C6H11)2]. *J. Organomet. Chem.* **2002**, *643−644*, 307−312.

(27) Suwanboon, S.; Amornpitoksuk, P.; Haidoux, A.; Tedenac, J. C. Structural and Optical Properties of Undoped and Aluminium Doped Zinc Oxide Nanoparticles via Precipitation Method at Low Temperature. *J. Alloys Compd.* **2008**, *462*, 335−339.

(28) Bahadur, S.; Sunkara, C. Effect of Transfer Film Structure, Composition and Bonding on the Tribological Behavior of Polyphenylene Sulfide Filled with Nanoparticles of TiO2, ZnO, CuO and SiC. *Wear* **2005**, *258*, 1411−1421.

(29) Diez-Pascual, A. M.; Naffakh, M. Inorganic Nanoparticle-Modified Carbon Fiber Fabric/Poly(phenylene sulphide) Laminates with Enhanced Thermomechanical Behaviour. *Materials* **2013**, *6*, 3171−3193.

(30) Abdolmaleki, A.; Mallakpour, S.; Borandeh, S. Effect of Silane-Modified ZnO on Morphology and Properties of Bionanocomposites Based on Poly(ester-amide) Containing Tyrosine Linkages. *Polym. Bull.* **2012**, *69*, 15−28.

(31) Colthup, N. B.; Day, L. H.; Wiberley, S. E. *Introduction to Infrared and Raman Spectroscopy*, 3rd ed.; Academic Press: San Diego, CA, 1990.

(32) AbdElhady, M. M. Preparation and Characterization of Chitosan/Zinc Oxide Nanoparticles for Imparting Antimicrobial and UV Protection to Cotton Fabric. *Int. J. Carbohydr. Chem.* **2012**, *2012*, 840591−840597.

(33) Xiang, T.; Yue, W. W.; Wang, R.; Liang, S.; Sun, S. D.; Zhao, C. S. Surface Hydrophilic Modification of Polyethersulfone Membranes by Surface-Initiated ATRP with Enhanced Blood Compatibility. *Colloids Surf., B* **2013**, *110*, 15−21.

(34) Alexander, L. E.; Krieger, R. E. *X-ray Diffraction Methods in Polymer Science*; Wiley: New York, 1969.

(35) Huang, Z. X.; Tang, Z. A.; Yu, J.; Bai, S. Thermal Conductivity of Nanoscale Polycrystalline ZnO Thin Films. *Physica B* **2011**, *406*, 811−823.

(36) Naffakh, M.; Diez-Pascual, A. M.; Marco, C.; Ellis, G. Morphology and Thermal Properties of Novel Poly(phenylene sulfide) Hybrid Nanocomposites Based on Single-walled Carbon Nanotubes and Inorganic Fullerene-like WS2 Nanoparticles. *J. Mater. Chem.* **2012**, *22*, 1418−1425.

(37) Gonzalez-Dominguez, J. M.; Castell, P.; Bespin-Gascon, S.; Anson-Casaos, A.; Diez-Pascual, A. M.; Gomez-Fatou, M. A.; Benito, A. M.; Maser, W. K.; Martinez, M. T. Covalent Functionalization of MWCNTs with Poly(p-phenylene sulphide) Oligomers: a Route to the Efficient Integration Through a Chemical Approach. *J. Mater. Chem.* **2012**, *22*, 21285−21297.

(38) van Krevelen, D. W. Some Basic Aspects of Flame Resistance of Polymeric Materials. *Polymer* **1975**, *16*, 615−620.

(39) Sanchez-Garica, M. D.; Langaron, J. M.; Hoa, S. V. Effect of Addition of Carbon Nanofibers and Carbon Nanotubes on the Properties of Thermoplastic Biopolymers. *Compos. Sci. Technol.* **2010**, *70*, 1095−1105.

(40) Schwartz, C. J.; Bahadur, S. Studies on the Tribological Behavior and Transfer Film−Counterface Bond Strength for Polyphenylene Sulfide Filled with Nanoscale Alumina Particles. *Wear* **2000**, *237*, 261−273.

(41) Kucheyev, S. O.; Bradby, J. E.; Williams, J. S.; Jagadish, C.; Swain, M. V. Mechanical Deformation of Single-Crystal ZnO. *Appl. Phys. Lett.* **2002**, *80*, 956−958.

(42) Adam, J.; Korneliusz, B. A.; Agnieszka, M. Dynamic Mechanical Thermal Analysis of Biocomposites Based on PLA and PHBV-a Comparative Study to PP Counterparts. *J. Appl. Polym. Sci.* **2013**, *130*, 3175−3183.

(43) Murayama, T. *Dynamic Mechanical Analysis of Polymeric Materials*, 2nd ed.; Elsevier: Amsterdam, 1978.

(44) Diez-Pascual, A. M.; Naffakh, M.; González-Domínguez, J. M.; Ansón, A.; Martínez-Rubi, Y.; Martínez, M. T.; Simard, B.; Gomez, M. A. High Performance PEEK/Carbon Nanotube Composites Compatibilized with Polysulfones-II. Mechanical and Electrical Properties. *Carbon* **2010**, *48*, 3500−3511.

(45) Diez-Pascual, A. M.; Naffakh, M. Enhancing the Thermomechanical Behaviour of Poly(phenylene sulphide) Based Composites via Incorporation of Covalently Grafted Carbon Nanotubes. *Composites, Part A* **2013**, *54*, 10−19.

(46) Adachi, S. *Properties of Group-IV, III-V and II-VI Semiconductors*; John Wiley & Sons: Chichester, U.K., 2005.

(47) Friedrich, K.; Schlarb, A. K. In *Tribology of Polymeric Nanocomposites*, Briscoe, B. J., Ed.; Tribology and Interface Enginnering Series; Elsevier: Oxford, U.K., 2008; Vol. 55.

(48) Yu, L.; Yang, S.; Liu, W.; Xue, Q. An Investigation of the Friction and Wear Behaviors of Polyphenylene Sulfide Filled with Solid Lubricants. *Polym. Eng. Sci.* **2000**, *40*, 1825−1832.

(49) Chang, L.; Zhang, Z. Tribological Properties of Epoxy Nanocomposites: II. A Combinative Effect of Short Carbon Fiber and Nano-TiO$_2$. *Wear* **2006**, *260*, 869−878.

(50) Diez-Pascual, A. M.; Naffakh, M.; Marco, C.; Ellis, G. Rheological and Tribological Properties of Carbon Nanotube/Thermoplastic Nanocomposites Incorporating Inorganic Fullerene-Like WS$_2$ Nanoparticles. *J. Phys. Chem. B* **2012**, *116*, 7959−7969.

(51) Ku, C.; Liepins, R. *Electrical Properties of Polymers*; Hanser: NewYork, 1987.

(52) Velayutham, T. S.; Majid, W. H. A.; Gan, W. C.; Zak, A. K.; Gan, S. N. Theoretical and Experimental Approach on Dielectric Properties of ZnO Nanoparticles and Polyurethane/ZnO Nanocomposites. *J. Appl. Phys.* **2012**, *112*, 54106−54116.

(53) Gupta, S. K. *Krishańs Engineering Physics*, 7th ed.; Bala, M., Ed.; Krishna Prakashan Media: Meerut, India, 2010; Vol. 2.

(54) Brayner, R.; Ferrari-Iliou, R.; Brivois, N.; Djediat, S.; Benedetti, M. F.; Fievet, F. Toxicological Impact Studies Based on Escherichia Coli Bacteria in Ultrafine ZnO Nanoparticles Colloidal Medium. *Nano Lett.* **2006**, *6*, 866−870.

(55) Heinlaan, M.; Ivask, A.; Blinova, I.; Dubourguier, H. C.; Kahru, A. Toxicity of Nanosized and Bulk ZnO, CuO and TiO$_2$ to Bacteria Vibrio Fischeri and Crustaceans Daphnia Magna and Thamnocephalus Platyurus. *Chemosphere* **2008**, *71*, 1308−1316.

(56) Tam, K. H.; Djurišić, A. B.; Chan, C. M. N.; Xi, Y. Y.; Tse, C. W.; Leung, Y. H.; Chan, W. K.; Leung, F. C. C.; Au, D. W. T. Antibacterial Activity of ZnO Nanorods Prepared by a Hydrothermal Method. *Thin Solid Films* **2008**, *516*, 6167−6174.